Soils and Rocks
An International Journal of Geotechnical and Geoenvironmental Engineering
www.soilsandrocks.com
ISSN 1980-9743
ISSN-e 2675-5475

Linear elastic fracture mechanics applied to rocks employing the Continuum Voronoi Block Model (CVBM)

Carlos Andrés Boada Becerra[1#], Leandro Lima Rasmussen[1]

Article

Keywords
Linear elastic fracture mechanics
Mode I fracture toughness
Stress concentration
Continuum Voronoi Block Model
Fracture propagation in rocks

Abstract

During fracture propagation in quasi-brittle materials such as rock, stress concentration plays a critical role as a result of stress redistribution, leading to elevated stress levels near crack tips. In classical elastic analytical solutions, stresses at the crack tip tend toward infinity; therefore, conventional elastic analyses are inadequate for describing fractured materials. This study employs Linear Elastic Fracture Mechanics (LEFM) to model this phenomenon in rock, with a focus on representing mode I fracture toughness (K_{Ic}). To address these processes, the Continuum Voronoi Block Model (CVBM) is utilized. CVBM is a pseudo-discontinuum approach implemented within a Finite Element Analysis (FEA) framework, combining Voronoi tessellation and the Goodman joint, to represent the rock's mesoscale structure. The model is first calibrated for deformational properties and tensile strength, and then iteratively adjusted to reproduce experimental K_{Ic} values. The calibration is validated under different boundary conditions through numerical simulations of Center-Cracked Tension (CCT) tests, Cracked Straight-Through Brazilian Disc (CSTBD) tests, and Semi-Circular Bending (SCB) tests, successfully reproducing fracture paths and yielding K_{Ic} values consistent with the literature.

1. Introduction

Rock is arguably one of the most complex natural materials. It is shaped by geological processes over millions of years and characterized by fractures spanning multiple scales (Fairhurst, 2013). This prolonged evolution results in a material with structural and mechanical behaviors that differ fundamentally from those of conventional engineering materials. Fracture propagation within rock involves the progressive failure of rock bridges. These bridges ultimately coalesce into continuous fractured surfaces, leading to the overall failure of the rock mass.

Traditional modeling approaches typically rely on continuum mechanics, which assume homogeneous stress distributions and material behavior. However, these models often fail to capture the heterogeneous stress fields in fractured rock masses, where micro- and macro-scale features interact. As a result, they may fail to reproduce realistic fracture surface geometries and often misestimate failure stresses.

Fracture phenomena in such materials have traditionally been addressed using Linear Elastic Fracture Mechanics (LEFM). This is a theory that simplifies the modeling of fracture propagation by assuming that the material behaves elastically, except at the crack tip where stress singularities and fracture initiation occur (Bazant & Planas, 1998). LEFM has proven effective in analyzing brittle materials and has also been extended to quasi-brittle materials such as rock and concrete.

In this study, fracture propagation in rock materials is simulated using the CVBM. CVBM is a pseudo-discontinuum approach that employs Voronoi tessellation and Goodman joints to replicate the rock's mesoscale heterogeneity. This paper proposes a calibration procedure to reproduce the mechanical behavior of the material at the laboratory scale, accounting for deformability, tensile strength, and mode I fracture toughness.

The calibrated model is then validated under different boundary conditions to assess its ability to simulate fracture propagation under varied loading scenarios. These include the Center Cracked Tension (CCT) test, the Cracked Straight-Through Brazilian Disc (CSTBD) test, and the Semi-Circular Bending (SCB) test – all of which are standard configurations for investigating mode I fracture propagation.

2. Theoretical background

In pseudo-discontinuum approaches such as the CVBM, the mechanical properties of the material are not directly prescribed. Instead, they emerge from the interaction between the model's constituent elements.

[#]Corresponding author. E-mail address: caboadab@unal.edu.co
[1]Universidade de Brasília, Departamento de Engenharia Geotécnica, Brasília, DF, Brasil.

Submitted on July 31, 2025; Final Acceptance on February 3, 2026; Discussion open until August 31, 2026.
Editor: Renato P. Cunha
https://doi.org/10.28927/SR.2026.011925

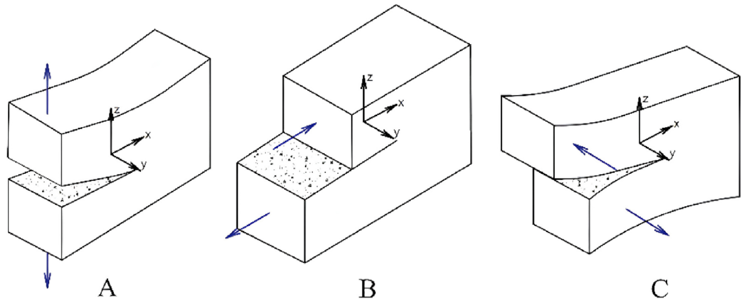

Figure 1. Schematic illustration showing the three fundamental modes of fracture propagation. (A) Mode I – opening or tensile mode; (B) Mode II – in-plane shear or sliding mode; (C) Mode III – out-of-plane shear or tearing mode.

Within the CVBM framework, both deformational and strength characteristics result from the combined influence of joint mechanical behavior and block geometry.

This chapter discusses how particle-based models offer a convenient platform for incorporating the principles of LEFM, where particle size becomes a critical parameter governing fracture behavior. The chapter reviews the fundamental concepts of LEFM. It then provides an in-depth discussion of the variables and mechanisms in the CVBM approach.

2.1 Linear elastic fracture mechanics

LEFM is a theoretical framework that analyzes the interaction of open cracks in elastic bodies. It is a simplified model, applicable under specific conditions. The primary assumption is that the material behaves elastically throughout its domain, except in the immediate vicinity of the crack tip. At this location, stress concentration causes localized inelastic behavior, which turn in governs the crack propagation process.

For materials to which this theory applies, the inelastic zone adjacent to the crack tip is small relative to the overall dimensions of the body and the crack length. This small zone justifies the simplification of assuming linear elastic behavior in nearly the entire domain. This condition is especially valid for brittle materials, where the inelastic region is extremely limited (Bazant & Planas, 1998).

LEFM defines three fundamental modes of crack propagation, illustrated in Figure 1.

The three fracture propagation configurations impose distinct stress states on the specimen. Fracture propagation begins once a critical condition is reached. This critical condition is further discussed in the following section.

2.2 Stress concentration phenomena

In a fractured and elastic body, stresses redistribute themselves, as illustrated in Figure 2. This redistribution is characterized by a stress relief zone along the fracture surfaces and a stress concentration region near the fracture tip. Inglis' (1913) solution (as cited in Bazant & Planas, 1998), demonstrates that a singularity occurs at the fracture tip. This phenomenon causes stress to approach infinity.

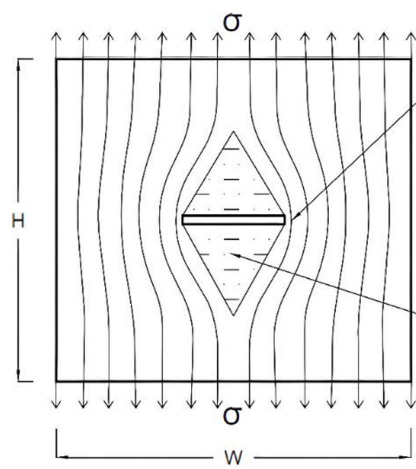

Figure 2. Stress re-distribution in fractured materials.

This interpretation indicates that conventional failure criteria, such as ultimate tensile strength, are inadequate for characterizing fractured materials. To address this limitation, Griffith (1921, 1924) (as cited in Bazant & Planas, 1998), developed an energy-based approach to describe the fracture process. Irwin (1957), later reformulated this framework in terms of stress, introducing the concept of the Stress Intensity Factor (SIF) (Bazant & Planas, 1998).

Within the SIF approach, applying a load to a fractured body alters the internal stress distribution, which in turn influences the SIF. As loading continues, SIF increases and may eventually reach a critical value that is intrinsic to the material. This value, known as fracture toughness, represents a limiting threshold beyond which fracture propagation occurs. Consequently, it serves as a fundamental criterion for fracture propagation, such as:

If $K_I < K_{Ic}$, no fracture propagation occurs.

If $K_I = K_{Ic}$, the system is in a quasi-static state.

If $K_I > K_{Ic}$, the fracture propagates.

In this study the critical value K_{Ic} was numerically calibrated, and three test configurations were modeled to

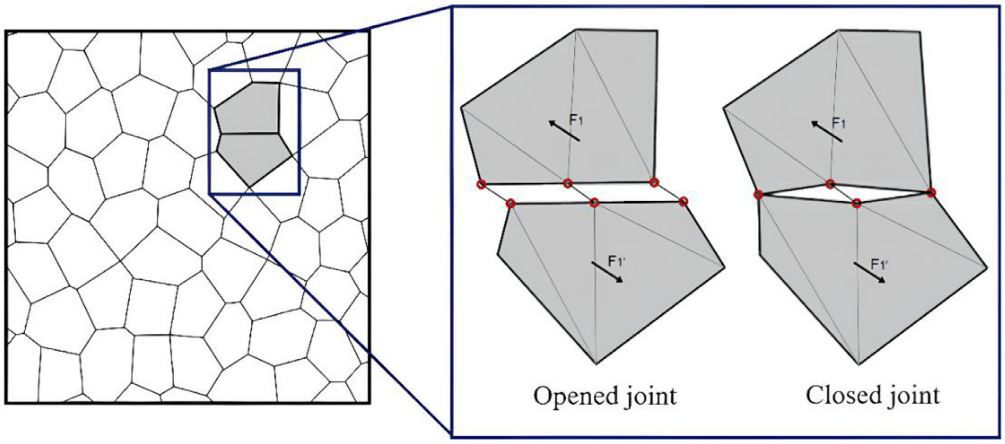

Figure 3. Voronoi tessellation geometry of medium regularity defined by open or closed joints from the RS2 CVBM.

determine the material's fracture toughness: the CCT test, the CSTBD test, and the SCB test. The mode I fracture toughness for each configuration, was then calculated using numerically derived equations from the literature.

2.3 Continuum Voronoi Block Model (CVBM)

The CVBM is a pseudo-discontinuum approach that captures the mesoscale structure of materials. It is also known as the Voronoi Tessellation Model (VTM) or Continuum Grain-Based Model (CGBM). The model uses Voronoi tessellation to generate a network of blocks and joints. Within the RS2 finite element software, this model incorporates Discrete Fracture Networks (DFN) to partition a continuous medium into polygonal blocks, which are interconnected by Goodman joints.

Figure 3 illustrates the model's conceptual framework, depicting a configuration with intermediate regularity and a mix of open and closed joints.

These zero-thickness, finite-length joints – defined by normal and shear stiffness parameters – govern the relative displacement between blocks and, consequently, influence the macroscopic deformability of the material. Depending on the modeling objectives, joints may be assigned either open or closed conditions. The software RS2 allows users to configure the Voronoi tessellation using parameters such as block size, density, and geometric regularity.

The generation of the Voronoi geometry in the CVBM tessellation model begins with a set of seed points, randomly distributed across the plane. Each polygon in the resulting tessellation is then associated with one of these seed points. The domain of each seed point is defined by the average distance calculation: every point within the domain of a nucleus i is closer to it than to any other nucleus j. This results in convex polygons that fill the entire space (Bolander & Saito 1998). Figure 4 presents an illustrative diagram of the tessellation structure generation process.

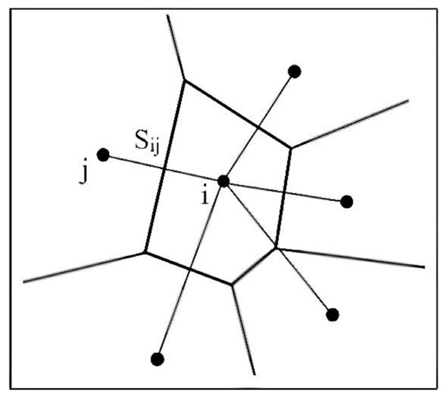

Figure 4. Voronoi tessellation generation algorithm diagram (modified – Bolander & Saito, 1998).

The model's tessellation, combined with its finite element structure and implicit integration scheme, provides remarkable computational efficiency. This efficiency is particularly notable when compared to other methodologies, such as the Discrete Element Method (DEM). Several studies have highlighted this advantage (Valderrama et al., 2024; Sanipour et al., 2022; Hamediazad & Bahrani, 2022; Soares et al., 2022; and Li & Bahrani, 2021). Furthermore, studies on underground works with high i-values the contacts are based in in-situ stress conditions show that the model yields promising results (Satheesh et al., 2024; Hamediazad & Bahrani, 2022).

In the CVBM, both the joints and the blocks contribute to the overall mechanical behavior of the material. To simplify the analysis and reduce the number of variables, the blocks are typically assumed to behave as rigid, elastic bodies. Within this framework, the material's deformation and strength are predominantly governed by the mechanical properties of the joints.

2.4 Grain based models and linear elastic fracture mechanics

Grain-based models (GBM) are a class of numerical approaches that represent the granular structure of materials in order to capture, among other features, their mechanical behavior. The CVBM belongs to this category; however, unlike other similar models, it is implemented within a finite element analysis (FEA) framework. This characteristic grants the model greater computational efficiency when compared to traditional discrete element methods (DEM).

Potyondy & Cundall (2004) and Rasmussen (2021) describe a correlation between grain size and mode I fracture toughness. Potyondy & Cundall (2004) demonstrated this relationship using a material composed of a perfectly cubic arrangement of spherical particles. By applying the LEFM principles and stress concentration theory the relationship expressed in Equation 1 is derived,

$$K_{Ic} = \sigma_t^{'} \sqrt{\pi R} \quad (1)$$

Equation 1 shows that for a fixed tensile strength; a specific fracture toughness can be defined by varying the particle radius. In the context of GBM, this implies that grain size becomes a controlling variable in the definition of mode I fracture toughness. This study tests this principle within the CVBM framework. Furthermore, it proposes a calibration algorithm to determine the appropriate mode I fracture toughness based on the grain size.

3. Calibration

3.1 Calibration algorithm

As outlined in Section 2.3, the mechanical properties of the CVBM arise from the interaction between blocks and joints. When the blocks are assumed to be rigid and elastic, the overall resistance and deformation of the body at the macro scale are governed exclusively by the characteristics of the joints. In this study, this assumption was adopted. The Mohr-Coulomb resistance criterion was applied, and both normal and shear stiffness were considered to calibrate the deformational parameters E (Young's modulus) and ν (Poisson's ratio).

In Figure 5 the suggested calibration algorithm is shown.

In the iterative calibration process, computational limitations restrict the use of a large number of elements. Simultaneously, the inherent variability of GBM necessitates a minimum number of elements within the cross-section to control the dispersion of the material behavior. Studies such as those conducted by Potyondy & Cundall (2004), Li & Bahrani (2021), and Sanipour et al. (2022) recommend that sample sizes ensure at least 10 element units along the smallest dimension of the specimen, in order to minimize the influence of block-scale variability on the overall mechanical response.

Accordingly, to maintain a sufficient number of elements in the cross-section and ensure the feasibility of specimens at different scales, specimens were evaluated following the scaling of the Voronoi block size. This approach ensured that, throughout the calibration process, the number of Voronoi blocks within the cross-section remained between 20 and 25, striking a balance between computational efficiency and result consistency.

3.2 Calibration tests

As illustrated in Figure 5, three test models were employed for material calibration. The first, the Unconfined Standard Compression (USC) test, was used to calibrate the deformational parameters: Young's modulus (E) and Poisson's ratio (ν). These properties are controlled through the joint stiffness parameters – normal stiffness (K_n) and shear stiffness (K_s). The absolute values of K_n and K_s are directly correlated with Young's modulus (E), while the K_n/K_s ratio

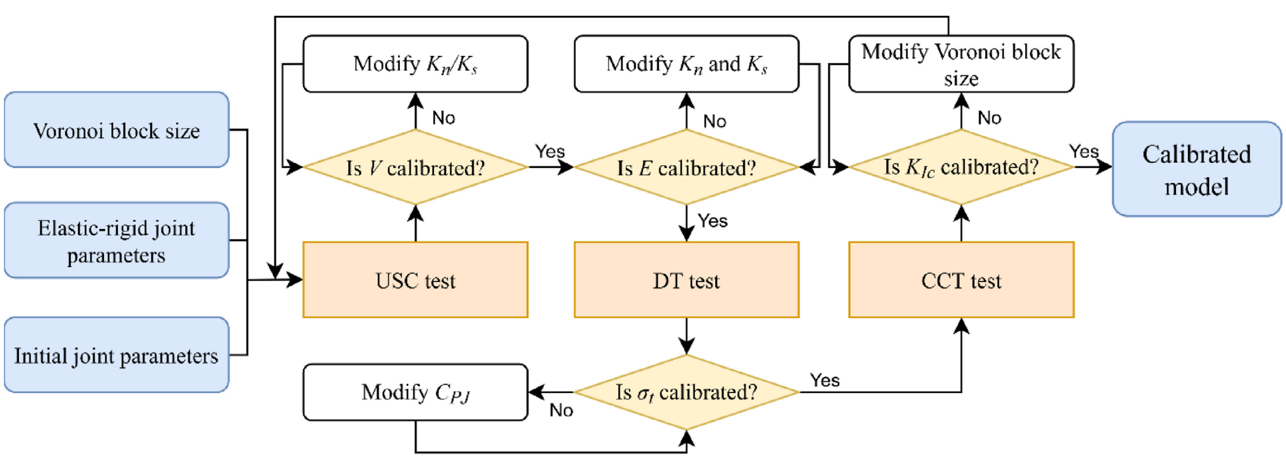

Figure 5. Suggested algorithm for CVBM calibration considering deformability, tensile resistance, and fracture toughness in mode I.

governs the Poisson's ratio (v), as it influences the volumetric deformation behavior of the material.

Subsequently, the direct tensile (DT) test was employed to define the tensile strength of the material. In RS2, joints can be defined using various failure criteria; in this study, the Mohr–Coulomb criterion was adopted. This criterion defines the strength envelope based on the friction angle (ϕ'), cohesion (c'), and tensile strength (σ_t). To avoid joint re-constitution – a phenomenon observed and described by Soares et al. (2022) when applying the Mohr–Coulomb criterion to CVBM joints – the tensile cut-off parameter was assigned a high value, thereby eliminating its influence from the failure envelope. Consequently, the strength behavior is governed exclusively by the ϕ' and c'.

The final test used to determine the material's mode I fracture toughness was the CCT test, with the geometry illustrated in Figure 6. In this configuration, a remote tensile stress σ is applied, causing stress to redistribute around a central notch in the specimen. This leads to crack propagation under mode I, driven by stress concentration at the crack tip.

To calculate the material's mode I SIF, Equation 2 developed by Tada (2000) was employed. When σ reaches a critical value and uncontrolled fracture propagation occurs, the K_I becomes K_{Ic}, which is a material property.

$$K_I = \sigma\sqrt{\pi a}\left[\sec\left(\frac{\pi a}{2W}\right)^{\frac{1}{2}}\right]\left[\begin{array}{c}1-0.025\left(\frac{a}{W}\right)^2+\\ 0.06\left(\frac{a}{W}\right)^4\end{array}\right] \quad (2)$$

The proposed algorithm is applied iteratively by varying the Voronoi block size. The relationship described in Equation 1 can be verified by plotting a graph of K_{Ic} versus Voronoi size. This graph facilitates the identification of the appropriate Voronoi size corresponding to a target K_{Ic}, thereby guiding the fracture toughness calibration process.

3.3 Calibration process

The material selected for representation in the calibration process was Lac du Bonnet granite (LdBG), which has been extensively utilized in research, including studies conducted by Lan et al. (2010), Ghazvinian et al. (2014), Soares et al. (2022) and Rasmussen & Min (2024). A comprehensive characterization of this material was carried out by Martin (1994); were considered in the calibration process, the reference values are presented in Table 1.

During the initial stage of the calibration process, a fixed K_n/K_s ratio of 3.4 was found to correspond to the required Poisson's ratio (v). This ratio remained consistent across subsequent iterations. Figure 7 presents the K_n and K_s values adopted for each Voronois block size tested during the calibration process.

As can be seen in the Figure 7, for smaller Voronoi block sizes, the normal and shear stiffness tend to be higher for a stablished Young Modulus and Poisson coefficient. This can be attributed to the high concentration of joints per unit area, which increases their influence on the macroscopic deformation of the material. This effect is reduced as the Voronoi block size increases, since this also reduces the joint density and, consequently, the influence of joints on the deformability properties.

The tensile strength was calibrated by adjusting the peak joint cohesion, and the fracture toughness was subsequently evaluated. Figure 8 illustrates the relationship identified between fracture toughness and Voronoi block size, in accordance with the relationship described in Equation 1.

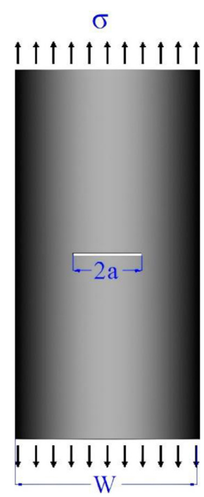

Figure 6. Center cracked tension test scheme with geometry definition parameters.

Table 1. LdBG parameters employed as references in the calibration process Martin (1994).

Mechanical parameter	Value	Standard deviation	n
Young modulus [GPa]	69.0	±5.8	81
Poisson coefficient	0.26	±0.04	81
Peak Tensile strength [MPa]	6.9	-	-
Fracture toughness (K_{Ic}) [MPa.m0,5]	1.82	±0.08	5
Friction angle [°]	59	-	-
Cohesion [MPa]	30	-	-

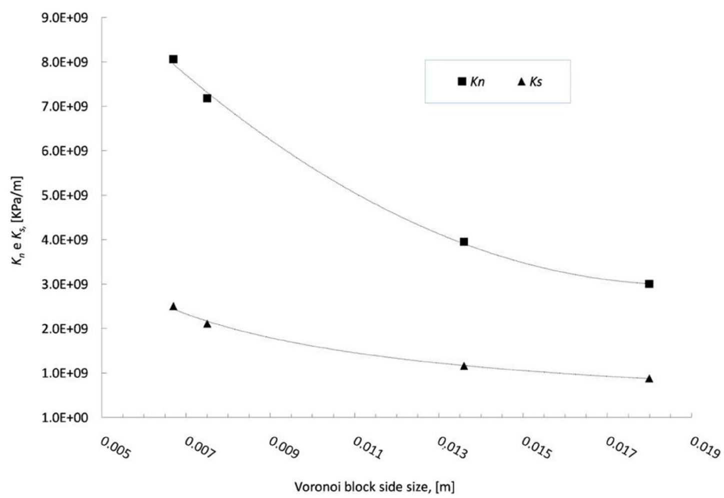

Figure 7. Normal and shear stiffness versus the Voronois sizes tested.

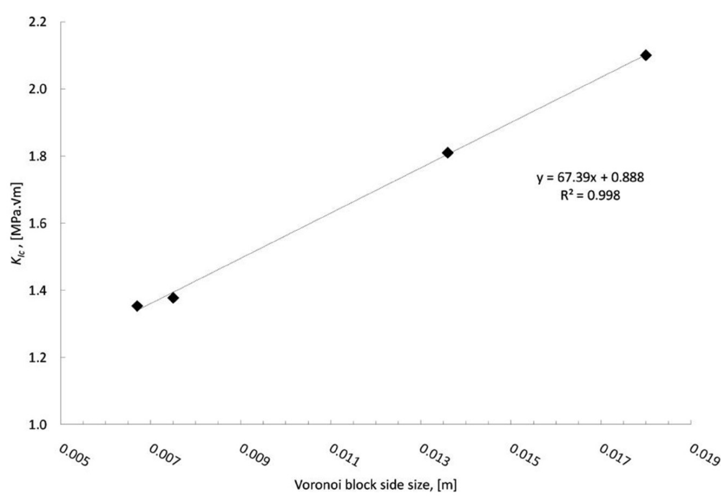

Figure 8. The relation between the fracture toughness and the Voronoi block size observed during the calibration process using CVBM.

The material behavior obtained, as shown in Figure 8, indicates a direct relationship between the Voronoi block side length and the fracture toughness, as expected from Equation 1. A linearization was applied to estimate the corresponding Voronoi block side length.

Based on the established relationship, a Voronoi block size of 0.00136 m was defined as adequate to represent the material fracture toughness of 1.82 MPa/m$^{0.5}$. With this Voronois size definition, the evaluation of mode I fracture toughness was made employing the CCT test. The mode I fracture toughness obtained in the test was calculated using Equation 2, considering a sample composed of five specimens with different Voronoi blocks arrays of the was K_{Ic} = 1.79 MPa.m$^{0.5}$ ± 0.09 MPa.m$^{0.5}$.

4. Results

4.1 Calibration results

The deformability and resistance characterization parameters obtained in the calibration process are compared with the objective values in Table 2.

The parameters employed to obtain the described deformational characteristics are presented in Table 3.

The obtained fracture surface – obtained with the parameters listed in Table 3 – employing CCT test is shown in Figure 9.

As can be seen, the fracture surface is a continuous plane, aligned with the original notch, as waited from the

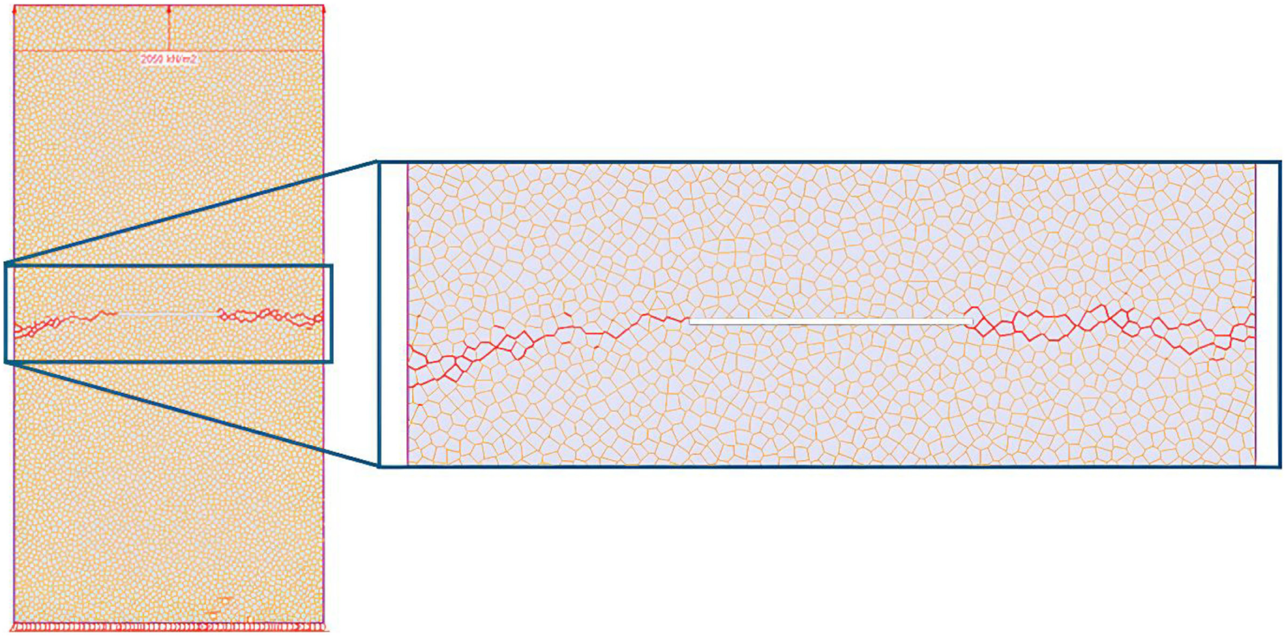

Figure 9. Fracture surface obtained in CCT test, obtained with the calibrated material using CVBM.

Table 2. Lac du Bonnet granite mechanical parameters compared with obtained through material modeling employing CVBM.

Mechanical parameter	Laboratorial Value	Standard deviation	n	Model obtained parameter value	Desv. Est.	n
Young's modulus [GPa]	69.0	±5.8	81	69.1	±0.4	5
Poisson coefficient	0.26	±0.04	81	0.263	±0.003	5
Peak tensile strength [MPa]	6.9	-	-	6.90	±0.07	5
Mode I Fracture toughness [MPa.m$^{0.5}$]	1.82	±0.08	5	1.79	±0.09	5

mode I fracture propagation. As described previously, though this methodology was obtained a K_{Ic} of 1.79 MPa.m$^{0.5}$ ± 0.09 MPa.m$^{0.5}$, which is an acceptable value with respect the calibration reference value of 1.82 MPa.m$^{0.5}$ ± 0.08 MPa.m$^{0.5}$.

In the next section, other boundaries conditions are tested to verify the mode I fracture toughness performance of the CVBM.

4.2 Verification under other boundaries conditions

The calibrated material was tested using the CCT to estimate its mode I fracture toughness. In this section, additional boundary conditions are evaluated to further investigate the material's fracture behavior. Two different tests were conducted. The first one, the SCB test, induces fracture propagation by flexural loading of a semicircular specimen. The second test employed was the CSTBD test. Its geometry boundaries conditions are presented in the Figure 10.

Equation 3 developed by Atkinson et al. (1982) (apud Omidimanesh et al., 2023) was used in this study to calculate the mode I fracture toughness for the boundary conditions of SCB test,

Table 3. Parameters employed to define the Lac du Bonnet granite model employing CVBM.

Parameter value	Voronoi blocks	Joints
Υ [kN/m^3]	26.7	-
v	0	-
E [kPa]	6.90E+17	-
Resistance criteria	**Elastic**	**Elastoplastic Mohr Coulomb**
K_n [kPa/m]	-	3.95E+09
K_s [kPa/m]	-	1,16E+12
σ_{Tpj} [kPa]	-	2.00E+20
C_{pj} [kPa]	-	13800
ϕ_{pj} [°]	-	45
σ_{Tr} [kPa]	-	0
C_{rj} [kPa]	-	0
ϕ_{rj} [°]	-	35

$$K_I = \left(\frac{P}{DB}\right)\sqrt{\pi a}\left(\begin{array}{c} -1.297+9.516\dfrac{s}{D}- \\ \left(0.47+16.457\dfrac{s}{D}\right)\left(\dfrac{2a}{D}\right)+ \\ \left(1.071+34.401\dfrac{s}{D}\right)\left(\dfrac{2a}{D}\right)^2 \end{array}\right) \quad (3)$$

Similarly, Equation 4, developed by Ke et al. (2008), was employed to calculate the mode I fracture toughness under the boundary conditions of the CSTBD test.

$$K_I = \frac{2P\sqrt{a}}{\sqrt{\pi}DB}F_I \quad ; \quad F_I = 1.343 \Leftrightarrow \frac{2a}{D} = 0.50 \tag{4}$$

This equation was obtained by experimental procedures, for the specific geometry relation of $\frac{2a}{D} = 0.50$ in which $F_I = 1.343$.

While the CCT test applies direct tension to the sample, the other boundary conditions lead the specimen to experience tensile stress through different mechanisms. The SCB test facilitates fracture propagation by flexural tensile stress, while the CSTBD test induces fracture through compressive loading. In this way, the three tests impose different conditions under which mode I fracture propagation occurs.

For modeling these tests, elastic joints – indicated in green – were used to prevent localized failure at the loading and support points, which are not accounted for in the analytical equations. The elastic properties of these regions were preserved to ensure proper stress transmission. The fracture surfaces resulting from the SCB and CSTBD tests are presented in Figure 11.

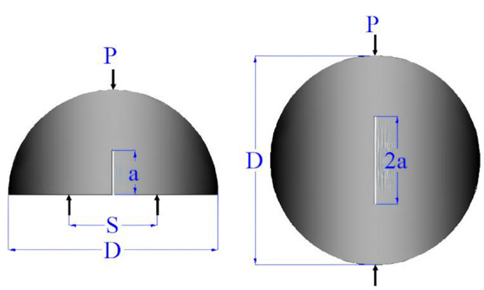

Figure 10. Semi circular bending test and cracked straight-though Brazilian disc boundary conditions.

The obtained value of mode I fracture toughness in SCB test was 1.75 MPa.m$^{0.5}$ ±0.08 MPa.m$^{0.5}$. Additionally, the value obtained in CSTBD was 1.76 MPa.m$^{0.5}$ ±0.07 MPa.m$^{0.5}$.

4.3 Mesh effect sensibility

The Voronoi blocks used in CVBM are implemented within the RS2 finite element software. Although the blocks are assumed to behave as rigid, high-stiffness elastic bodies to minimize their contribution to the overall deformation and fracture, this section evaluates whether the size of the finite elements within the blocks affects the fracture propagation toughness. To this, CCT tests were performed using triangular three-node finite element meshes with varying side lengths.

For the calibrated material, with Voronoi blocks having an average side length of 0.0136 m, it was observed that the coarsest mesh that could be employed contained elements of approximately 0.03 m in size. This was therefore adopted as the upper bound for comparison. The minimum element size evaluated was 0.01 m, as smaller sizes were deemed unnecessary for the problem at hand and impractical due to their high computational cost.

The fracture behavior and ultimate strength results for specimens using the same Voronoi network but different mesh densities are presented in Table 4.

Similar fracture propagation surfaces were observed for mesh sizes of 0.03 m, 0.02 m, and 0.015 m, with the corresponding fracture toughness values remaining consistent across these configurations. In contrast, the model with

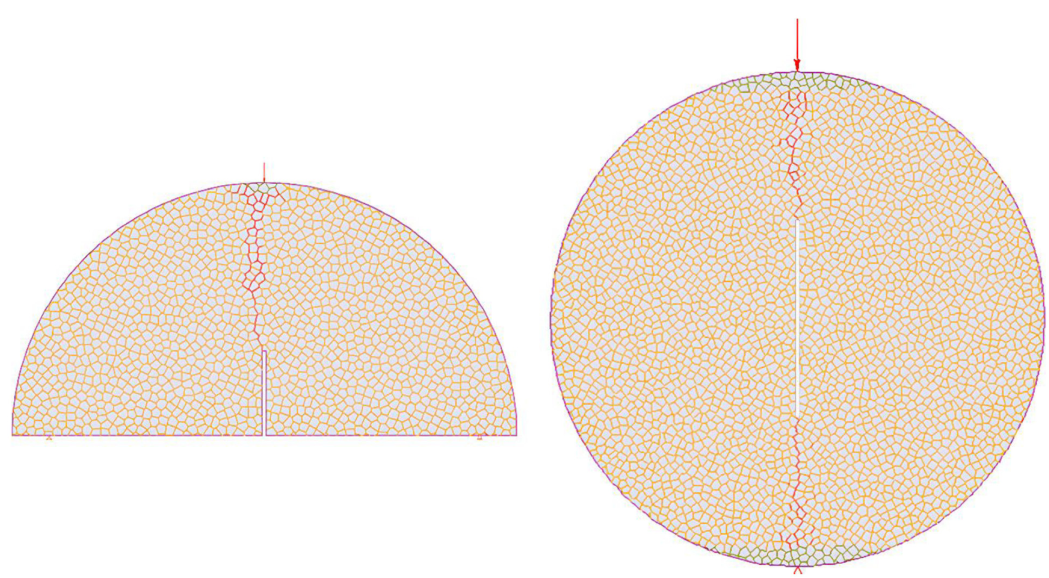

Figure 11. Fracture surfaces obtained with SCB and CSTBD test boundaries conditions.

Table 4. Dimensional analysis of finite elements size and fracture toughness.

Finite elements size [m]	K_{Ic} [MPa.m$^{0.5}$]	Propagated fracture surfaces
0.03	1.86	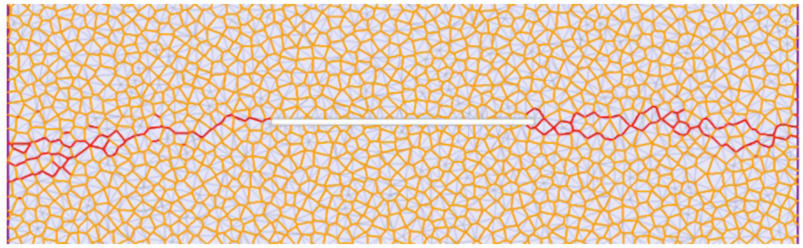
0.02	1.86	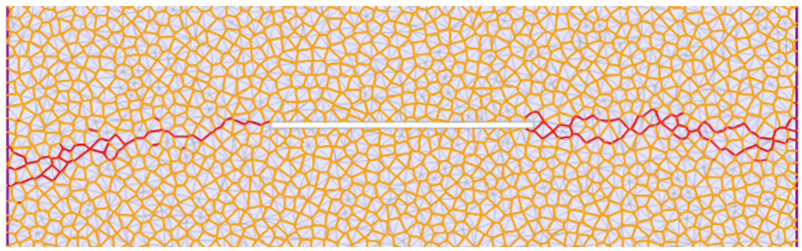
0.015	1.86	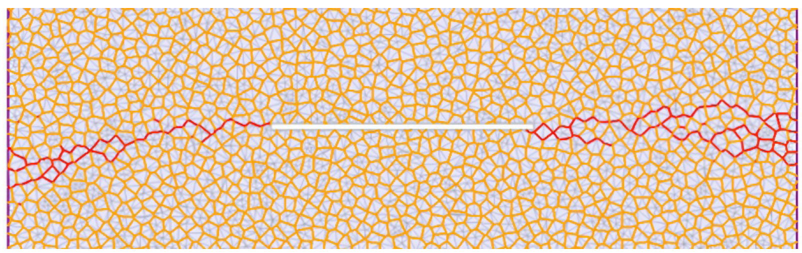
0.01	1.81	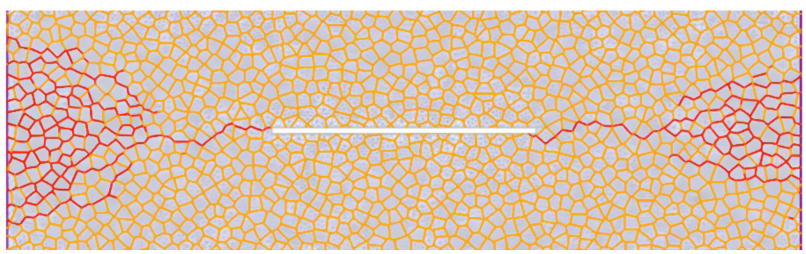

0.01 m finite elements exhibited a distinct fracture surface, characterized by broader propagation at the corners and a noticeable reduction in fracture toughness. These variations, however, are not considered a limitation, as such fine mesh sizes fall outside the scope of relevance for the objectives of the present study.

Given that the Voronoi blocks are discretized using finite elements, the maximum allowable element size is inherently limited by the average block dimensions. Although coarser meshes result in models that are computationally lighter and faster, they often lead to poor mesh quality and convergence issues due to the formation of slender or irregular elements. This issue can be mitigated by adopting an intermediate mesh density, which improves the regularity of the finite elements within the Voronoi blocks while maintaining computational efficiency. In the present study, a mesh size of 0.015 m was selected as it provides a balanced trade-off between numerical stability and performance.

5. Conclusion

The applicability of LEFM within the CVBM framework was successfully demonstrated. The mode I fracture toughness was consistently determined during the calibration process, which required four iterations to establish the representative grain size for the rock, referred to as LdBG. These results confirm that the proposed calibration algorithm is effective in reproducing the material's mechanical behavior, as it appropriately accounts for deformability, tensile strength, and fracture toughness (K_{Ic}).

Material performance was assessed using three modeled tests. The mode I fracture toughness values obtained were: K_{Ic} = 1.79 MPa.m$^{0.5}$ ± 0.09 MPa.m$^{0.5}$ for CCT, 1.75 MPa.m$^{0.5}$ ±0.08 MPa.m$^{0.5}$ for SCB, and 1.76 MPa.m$^{0.5}$ ±0.07 MPa.m$^{0.5}$ for CSTBD test. These results are consistent with one another, with the observed differences falling within the respective standard deviations, thereby validating the material's mode I fracture toughness under varying boundary conditions.

Other ways to improve the calibration procedures – such as better representation of the material under high confinement and the inclusion of mode II fracture toughness – must be explored. In this context, the use of pseudo-discontinuum methods within a finite element framework, such as the CVBM, can become a valuable tool for modeling fracture problems, especially considering their computational efficiency, which enables faster exploration of these possibilities.

The sensitivity of the fracture process to finite element size was evaluated, and the results demonstrated stability within the element sizes deemed appropriate for modeling. Although some differences were observed with the smallest element size considered, these variations are attributed to changes in the convergence behavior of the numerical algorithm, rather than an inherent sensitivity of the method to element size. Therefore, the CVBM can be regarded as robust with respect to finite element discretization in the context of fracture modeling.

As described throughout the paper, the imposed calibration criteria – deformation, tensile strength, and mode I fracture toughness – were tested. These considerations represent the behavior of the material under low-confinement tensile states, but they have not been validated or calibrated to represent higher stress states, including shear behavior. This condition limits the representativeness of the model.

Acknowledgements

The author gratefully acknowledges the support of the Brazilian National Council for Scientific and Technological Development (CNPq) for funding the master's studies at the University of Brasília through process number 164573/2022-4. Sincere thanks are also extended to the Brazilian people, whose commitment to national development makes academic research of this nature possible.

Declaration of interest

The authors have no conflicts of interest to declare. All co-authors have observed and affirmed the contents of the paper and there is no financial interest to report.

Authors' contributions

Carlos Andrés Boada Becerra: Conceptualization, Methodology, Models development, Data curation, Formal analysis, Visualization, Writing – original draft. Leandro Lima Rasmussen: Conceptualization, Methodology, Supervision, Validation, Project Administration.

Data availability

The datasets generated analyzed in the course of the current study are available from the corresponding author upon request.

Declaration of use of generative artificial intelligence

This work was prepared with the assistance of generative artificial intelligence (GenAI), specifically ChatGPT for MS Word, with the aim of grammar correction and translation. The entire process of using this tool was supervised, reviewed, and, when necessary, edited by the authors. The authors assume full responsibility for the content of the publication that involved the aid of GenAI.

List of symbols and abbreviations

s	Distance between support points.
B	Thickness of the test sample.
D	Diameter of the test sample.
F_I	Boundary factor used for a specific geometry rate.
K_I	Stress intensity factor in mode I.
K_{Ic}	Fracture toughness in mode I.
P	Punctual load.
R	Particle radius.
W	Width of the test sample.
a	Half of the initial notch length.
σ	Traction remotely imposed.
$\sigma_t^{'}$	Intact material tensile strength in macro-scale.

References

Atkinson, C., Smelser, R.E., & Sanchez, J. (1982). Combined mode fracture via the cracked Brazilian disk test. *International Journal of Fracture*, 18(4), 279-291. http://doi.org/10.1007/BF00015688.

Bazant, Z.P., & Planas, J. (1998). *Fracture and size effect in concrete and other quasibrittle materials*. Oxfordshire: Taylor & Francis.

Bolander Jr, J.E., & Saito, S. (1998). Fracture analyses using spring networks with random geometry. *Engineering Fracture Mechanics*, 61(5-6), 569-591. http://doi.org/10.1016/S0013-7944(98)00069-1.

Fairhurst, C. (2013). Fractures and fracturing: hydraulic fracturing in jointed rock. In: Jeffrey, R. (Ed.), *Proceedings of the ISRM International Conference for Effective and Sustainable Hydraulic Fracturing 2013* (pp. 47–79). London: InTech. http://doi.org/10.5772/56366.

Ghazvinian, E., Diederichs, M.S., & Quey, R. (2014). 3D random Voronoi grain-based models for simulation of brittle rock damage and fabric-guided micro fracturing. *Journal of Rock Mechanics and Geotechnical Engineering*, 6(6), 506-521. http://doi.org/10.1016/j.jrmge.2014.09.001.

Griffith, A.A. (1921). The phenomena of rupture and flow in solids. *Philosophical Transactions of the Royal Society of*

London. Series A, Containing Papers of a Mathematical or Physical Character, 221(582-593), 163-198. http://doi.org/10.1098/rsta.1921.0006.

Griffith, A. (1924). "The theory of rupture". In: C.B. Biereno, & J.M. Burgers (Eds.), *Proceedings of the First International Conference of Applied Mechanics* (pp. 55–63). Delft: Tech. Boekhandel en Drukkerij.

Hamediazad, F., & Bahrani, N. (2022). Simulation of hard rock pillar failure using 2D continuum-based Voronoi tessellated models: the case of Quirke Mine, Canada. *Computers and Geotechnics*, 148, 104808. http://doi.org/10.1016/j.compgeo.2022.104808.

Inglis, C.E. (1913). Stresses in a plate due to the presence of cracks and sharp corners. *Transactions of the Institution of Naval Architects*, 55, 219-241.

Irwin, G.R. (1957). Analysis of stresses and strains near the end of a crack traversing a plate. *Journal of Applied Mechanics – Transactions of the ASME*, 24, 361–364.

Ke, C.C., Chen, C.S., & Tu, C.H. (2008). Determination of fracture toughness of anisotropic rocks by boundary element method. *Rock Mechanics and Rock Engineering*, 41(4), 509-538. http://doi.org/10.1007/s00603-005-0089-9.

Lan, H., Martin, C.D., & Hu, B. (2010). Effect of heterogeneity of brittle rock on micromechanical extensile behavior during compression loading. *Journal of Geophysical Research*, 115(B1), 2009JB006496. http://doi.org/10.1029/2009JB006496.

Li, Y., & Bahrani, N. (2021). Strength and failure mechanism of highly interlocked jointed pillars: insights from upscaled continuum grain-based models of a jointed rock mass analogue. *Computers and Geotechnics*, 137, 104278. http://doi.org/10.1016/j.compgeo.2021.104278.

Martin, C.D. (1994). *The strength of massive Lac du Bonnet granite around underground openings [Report]*. Ottawa: National Library of Canada.

Omidimanesh, M., Sarfarazi, V., Babanouri, N., & Rezaei, A. (2023). Investigation of fracture toughness of shotcrete using semi circular bend test and notched Brazilian disc test: experimental test and numerical approach. *Journal of Mining and Environment*, 14, 233-242. http://doi.org/10.22044/jme.2022.12465.2263.

Potyondy, D.O., & Cundall, P.A. (2004). A bonded particle model for rock. *International Journal of Rock Mechanics and Mining Sciences*, 41(8), 1329-1364. http://doi.org/10.1016/j.ijrmms.2004.09.011.

Rasmussen, L.L. (2021). Hybrid lattice/discrete element method for bonded block modeling of rocks. *Computers and Geotechnics*, 130, 103907. http://doi.org/10.1016/j.compgeo.2020.103907.

Rasmussen, L.L., & Min, K.B. (2024). Hybrid lattice/discrete element analysis of spalling failure in rock tunnels. *Tunnelling and Underground Space Technology*, 153, 106034. http://doi.org/10.1016/j.tust.2024.106034.

Sanipour, S., Bahrani, N., & Corkum, A. (2022). Simulation of brittle failure around Canada's Mine-By experiment tunnel using 2D continuum-based Voronoi tessellated models. *Rock Mechanics and Rock Engineering*, 55(10), 6387-6408. http://doi.org/10.1007/s00603-022-02969-7.

Satheesh, P.V., Shirole, D., & Sinha, S. (2024). Investigation of the effect of confinement on intact Wombeyan marble using continuum grain-based model (CGBM). In: *58th U.S. Rock Mechanics/Geomechanics Symposium*, Golden, Colorado, USA.

Soares, E.R.S., Farias, M.M., & Rasmussen, L.L. (2022). The continuum Voronoi block model for simulation of fracture process in hard rocks. *International Journal for Numerical and Analytical Methods in Geomechanics*, 46(1), 89-112. http://doi.org/10.1002/nag.3292.

Tada, H. (2000). *The stress analysis of cracks handbook* (3rd ed.). New York: ASME eBooks. http://doi.org/10.1115/1.801535.

Valderrama, J.O., Assis, A.P., & Rasmussen, L.L. (2024). Brittle rock behavior simulation using heterogeneous pseudo-discontinuum model. *Computers and Geotechnics*, 173, 106474. http://doi.org/10.1016/j.compgeo.2024.106474.